

# Enhancing Connection Strength in Freeform Modular Reconfigurable Robots through Holey Sphere and Gripper Mechanisms

Peiqi Wang<sup>1,2</sup>, Guanqi Liang<sup>1,2,†</sup>, Da Zhao<sup>3</sup>, and Tin Lun Lam<sup>1,2,†</sup>

**Abstract**—Freeform modular self-reconfigurable robot (MSRR) systems overcome traditional docking limitations, enabling rapid and continuous connections between modules in any direction. Recent advancements in freeform MSRR technology have significantly enhanced connectivity and mobility. However, limitations in connector strength and operational efficiency in existing designs restrict performance. This paper proposes a rigid freeform connector and a rigid magnetic track design to improve the connection and motion performance of the SnailBot. Each SnailBot is equipped with a multi-channel rope-driven gripper, a metal spherical shell with densely distributed circular holes on the back, and a rigid chain design conforming to the spherical surface. This combination allows each SnailBot to move precisely along the surface of a peer, facilitated by the ferromagnetic spherical shell and magnetic track. The integration of the gripper and spherical shell hole array provides robust inter-module connections in any position and orientation. The effectiveness of these designs has been validated through a series of experiments and analyses, demonstrating improved connection and motion performance in the SnailBot dual-mode connector system and expanding its potential applications and functional capabilities.

## I. INTRODUCTION

Modular self-reconfigurable robot (MSRR) systems are composed of multiple independent modules that can be reconfigured and interconnected to form various configurations, enabling adaptation to diverse tasks and environments [1]. The primary advantage of MSRR systems lies in their high flexibility, adaptability, and capability to overcome complex terrains. Additionally, MSRR systems can alter their configuration according to specific task requirements, performing a wide range of operations, from object manipulation to transportation. The modular design of MSRR systems also confers significant scalability, ease of maintenance, and upgradeability, making them suitable for applications in exploration, rescue, and education, thereby exhibiting substantial potential for broad application.

The self-reconfigurable modular robots incorporate a novel connector design that facilitates unrestricted, rapid, and

This work was supported in part by the National Natural Science Foundation of China under Grant 62073274, in part by the Guangdong Basic and Applied Basic Research Foundation under Grant 2023B1515020089; and in part by the Shenzhen Institute of Artificial Intelligence and Robotics for Society under Grant AC01202101103.

<sup>1</sup>School of Science and Engineering, The Chinese University of Hong Kong, Shenzhen, China.

<sup>2</sup>Shenzhen Institute of Artificial Intelligence and Robotics for Society (AIRS), Shenzhen, Guangdong, 518172, P.R. China.

<sup>3</sup>Department of Mechanical and Automation Engineering, The Chinese University of Hong Kong, Hong Kong, China.

<sup>†</sup>Corresponding authors: Guanqi Liang and Tin Lun Lam. (e-mail: guanqiliang@link.cuhk.edu.cn; tllam@cuhk.edu.cn)

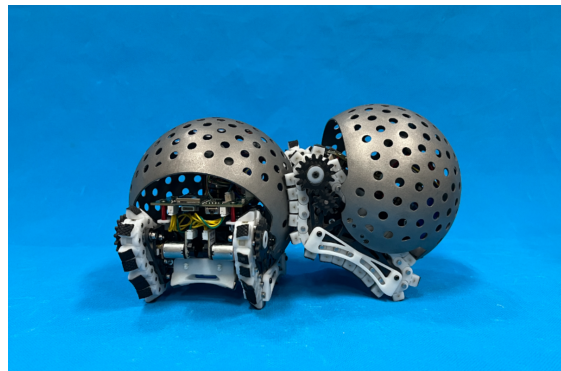


Fig. 1. A freeform MSRR system - SnailBot.

continuous connections between modules in any direction. Initially, freeform connectors were developed for 2D applications [2]–[4], offering some degree of flexibility, though their range of motion, connection capabilities, and degrees of freedom were constrained. With advancements in technology, 3D freeform MSRR systems, such as FreeBOT [5], [6] and FireAnt3D [7], have emerged. These systems overcome the limitations of traditional modular robots, which require specific connector alignments and precise docking procedures. The freeform surfaces in these advanced MSRR systems significantly enhance the dexterity of inter-module connections and movements, addressing challenges such as difficult docking, slow reconfiguration, and limited configuration options prevalent in conventional systems. However, the strength of inter-module connections directly affects the configuration capabilities of MSRR systems, and different types of connectors provide varying levels of connection force. Various connector designs, such as electromagnets [8]–[10], permanent magnets [11]–[13], mechanical hooks [14]–[18], binder material [19] and vacuum [20], have been applied in MSRR systems. Compared to other types of connectors, mechanical hooks generally offer stronger connection forces and good reusability. However, they often require specially designed connection surfaces and precise alignment during docking, which limits the flexibility of module connections. As a result, they are difficult to apply in freeform MSRR systems. Recent advancements in freeform MSRR systems have led to the development of heterogeneous truss designs [21], [22], spherical gear anti-slip structures [23], and biomimetic dual-mode connectors [24], further enhancing system connectivity and robustness. Nevertheless, they struggle to handle tasks requiring greater load-bearing capacity. Nevertheless, research on stronger connectors for freeform MSRR systems is still necessary.

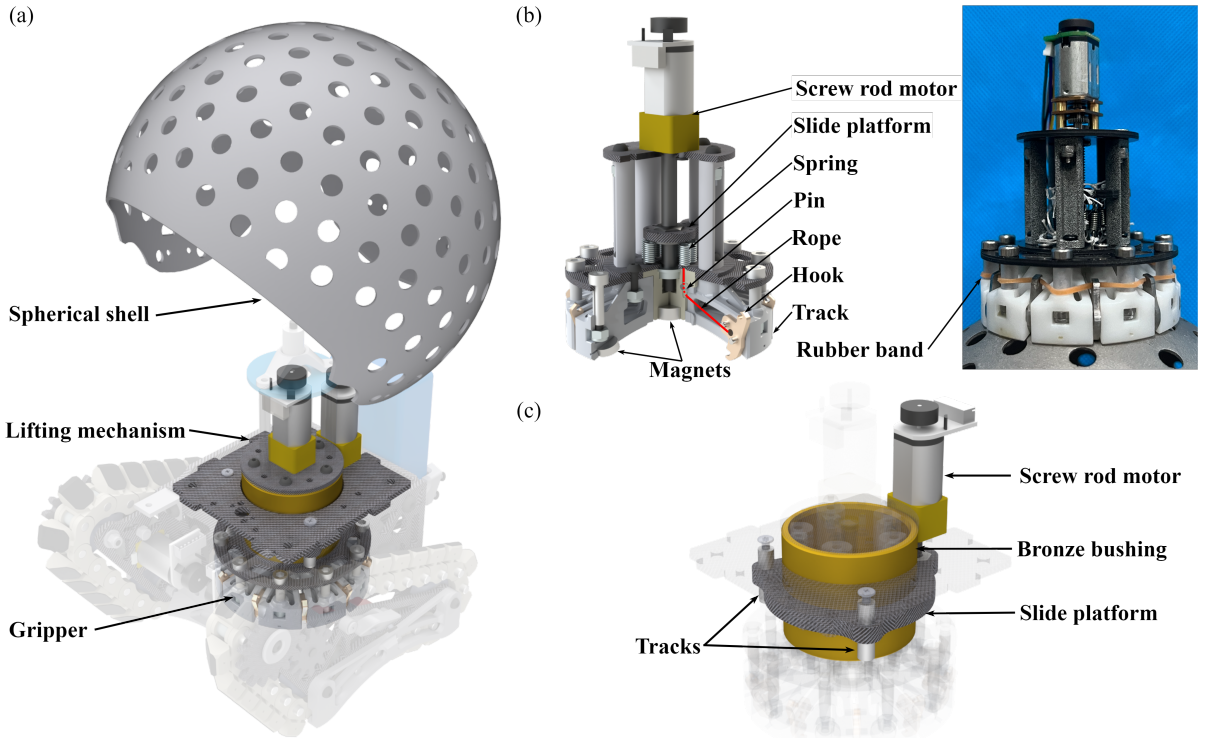


Fig. 2. (a) Describe the design of the spherical shell and the positional relationship between the gripper and the SnailBot. (b) This is a schematic diagram of the gripper structure. The spring is bound to the slide platform with a rope. The hook is fitted with two cylindrical pins. The outer ring magnets have a size of  $\phi 6 \times 2$ , and the center magnet has a size of  $\phi 8 \times 3$ . (c) Describe the structure of the lifting mechanism.

In previous work, the SnailBot design utilized a dual-mode connector system, featuring magnetic rubber tracks that enable modules to move independently across planes, outdoor environments, and even the surfaces of other modules, thereby enhancing reconfiguration capabilities and independent mobility. Concurrently, the suction cup connector strengthens inter-module connections, improving the overall manipulation capabilities of the assembled modules. However, in previous implementations, the suction cup connector's force was inadequate relative to the module's weight, limiting its effectiveness in various tasks. Moreover, the continuous operation of the suction cup motor proved inefficient, and the deformability of the magnetic rubber track resulted in poor surface fit on spherical structures. These limitations indicate that both the connector performance and magnetic track design in the previous iteration require optimization and engineering improvements.

In this paper, we propose a rigid freeform connector and a rigid magnetic track design to enhance the connection and mobility performance of the SnailBot. Each SnailBot is equipped with a multi-channel rope-driven gripper at the base, an spherical shell with densely distributed circular holes on the back, and a rigid chain design that conforms to the spherical surface. This combination allows each SnailBot to traverse the surface of a peer with high precision and connectivity, facilitated by the ferromagnetic spherical shell and magnetic track. Furthermore, the system achieves robust inter-module connections in any position and orientation through the integration of the gripper and spherical shell

hole array. The efficacy of these designs has been validated through a series of experiments and analyses, demonstrating improved connection and motion performance in the SnailBot dual-mode connector system, thereby expanding its potential applications and functional capabilities.

## II. RIGID FREEFORM CONNECTOR

Enhancing connection strength is particularly beneficial for more complex configurations. This section introduces a spherical rigid freeform connector designed to strengthen the inter-module connection force. The connector comprises two main components: a gripper and a spherical shell, with an additional lifting mechanism.

### A. Gripper

The basic mechanical structure of the gripper is depicted in Fig. 2(b). Each gripper is equipped with multiple hooks designed for gripping tasks. These hooks operate through a system of fine ropes and springs, mounted on a vertically moving sliding platform powered by a screw rod motor. The hooks move along tracks on both sides to ensure stable and guided motion. At the base of the gripper, magnets are installed to provide sufficient magnetic force, securing the gripper firmly to the spherical shell. The hooks' motion is controlled by rubber bands, with one end connected to the hook and the other facilitating its rotation and reset. As the sliding platform moves upward, the hooks follow the track, constrained by the track's design. If a hook cannot pass through a hole, the track's inner side limits its motion.

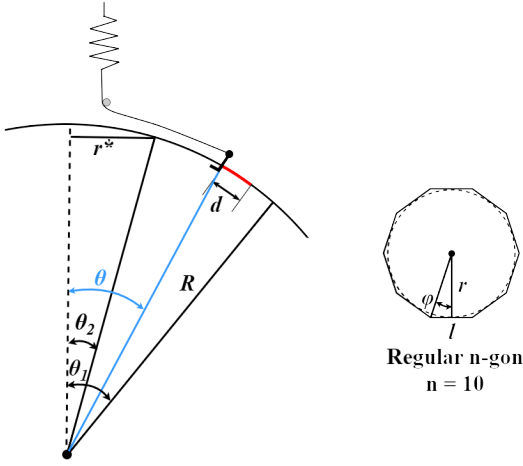


Fig. 3. Gripper-Spherical Shell geometric relationship

When a hook does pass through a hole, the rubber band drives its rotation, while a cylindrical shaft restricts the hook's rotational angle to ensure proper alignment. The gripper can engage with multiple holes at once, regardless of their spacing, with springs on the sliding platform providing adaptability.

Notably, the number and arrangement of hooks must ensure sufficient success in practical gripping applications. The design should minimize friction and resistance during hook movement to maintain operational flexibility and efficiency. Additionally, the configuration and force distribution of the magnets must be balanced to guarantee stable attachment to the spherical shell.

The design of the mechanical gripper is defined by key parameters, particularly the number of hooks and their range of motion. Here, we describe the method used to calculate the range of motion for the hooks. During the design process, random points are generated on the spherical surface, representing the projections of the gripper's central axis. By generating arcs in random directions within the defined angular range and distributing these arcs around the central axis, they are divided into  $n$  segments. If an arc passes through a hole, it is deemed valid. The gripper is considered successful if the number of valid arcs exceeds  $\lceil \frac{n}{2} \rceil$ , indicating that the design enables effective gripping. Additionally, the hooks are evenly distributed, and each hook must occupy a width of at least 5mm to ensure reasonable assembly and structural integrity, with  $l = 5$  mm. Assuming the gripper has  $n$  hooks, the angle between them is  $\varphi = \frac{180^\circ}{n}$ . The theoretical minimum radius  $r$  for the hook distribution is calculated as follows:

$$r = \frac{l}{2 \sin \varphi} \times \sin \left( \frac{\pi}{2} - \varphi \right) \quad (1)$$

Given that the diameter of the hole is  $d$ , the hook is considered effective if the arc it occupies comes within a distance less than  $d/2$  from the hole's center. On a spherical surface with a radius of  $R = 60$  mm, the shortest effective

distance  $r^*$  that a hook can reach is:

$$r^* = r + \frac{d}{2} \quad (2)$$

From this, the angular limit  $\theta_2$  for hook motion is derived as:

$$\theta_2 = \arcsin \left( \frac{r^*}{R} \right) \quad (3)$$

Thus, the motion range for a single hook is:

$$\theta \in (\theta_2, \theta_1) \quad (4)$$

The detailed calculation and determination of the number of hooks, aimed at optimizing the overall success rate of the clamping operation, will be presented in the following section.

### B. Spherical Shell

The design and production of the spherical shell and gripper mechanisms must adhere to three critical principles:

- Ensure even distribution of holes across the spherical shell's surface.
- Design the gripper to maximize grasping success while maintaining magnetic connectivity.
- Optimize the number of gripper hooks to balance performance and cost.

Achieving a uniform distribution of holes on the spherical shell is the first design challenge. To address this, a particle theory-based approach is employed. In this method, the surface of the sphere is modeled as a closed system of particles, where each particle represents a hole. These particles are treated as if they repel each other, similar to charged particles, resulting in a natural equilibrium state. This equilibrium ensures that the holes are evenly distributed across the surface of the spherical shell.

The design of the spherical shell, especially the layout and functionality of the surface hole array, plays a critical role in the connector. These holes not only determine the practical performance of the spherical shell within the connector but also influence its interaction with the gripper. The primary purpose of the shell's hole design is to provide multi-angle, multi-directional connection points in three-dimensional space, allowing the gripper to capture and secure the spherical shell from any direction. These holes must ensure smooth entry for the gripper and maintain stability after capture. Therefore, their arrangement is also influenced by mechanical factors, aiming for balanced force distribution during gripping. The surface of the spherical shell undergoes precise calculation and optimization to ensure that the arrangement and number of holes maximize the gripper's operation. For a unit spherical surface, randomly generating a point  $(x, y, z)$  gives the initial position vector  $r_i = [x, y, z]$ . For each pair of points  $r_i$  and  $r_j$ , the vector difference is calculated as

$$\mathbf{d}_{ij} = \mathbf{r}_i - \mathbf{r}_j \quad (5)$$

The distance  $L_{ij}$  is the magnitude of the vector difference.

$$L_{ij} = \|\mathbf{d}_{ij}\| = \sqrt{(x_i - x_j)^2 + (y_i - y_j)^2 + (z_i - z_j)^2} \quad (6)$$

Then, the repulsive force is calculated based on the distance between the points. Assuming the magnitude of the force is inversely proportional to the cube of the distance.

$$\mathbf{F}_i = \sum_{j \neq i} \frac{\mathbf{d}_{ij}}{L_{ij}^3} \quad (7)$$

Next, the radial component  $F_{r_i}$  and  $F_{v_i}$  the tangential component of the force are calculated.

$$\mathbf{F}_{r_i} = (\mathbf{F}_i \cdot \mathbf{r}_i) \mathbf{r}_i \quad (8)$$

$$\mathbf{F}_{v_i} = \mathbf{F}_i - \mathbf{F}_{r_i} \quad (9)$$

The position is updated by the current velocity and normalized. The initial velocity is 0.

$$\mathbf{r}_{i^*} = \frac{\mathbf{r}_i + \mathbf{v}_i}{\|\mathbf{r}_i + \mathbf{v}_i\|} \quad (10)$$

The velocity is updated based on the tangential component of the force.

$$\mathbf{v}_{i^*} = \mathbf{v}_i + G \cdot \mathbf{F}_{v_i} \quad (11)$$

where  $G$  is the repulsive force constant, controlling the step size of the velocity update. This is followed by the next generation calculation. Typically the total energy is used as an indicator to monitor convergence. Here the sum of distances between all points is used instead. It decreases with the number of iterations and eventually levels off. The positions are iteratively updated until uniform distribution is achieved. These evenly distributed points are then mapped onto the target diameter of the spherical surface, using them as the centers of the holes, resulting in the complete spherical shell.

The next step is to determine the optimal number of hooks ( $M$ ), the number of holes ( $N$ ) on the spherical shell, and the size of each hole ( $X$ ). This represents a multivariate optimization problem. These variables must be balanced to maximize the success rate of gripper attachment without compromising the mechanical properties of the spherical shell.

Our engineering experience shows that to maintain effective magnetic connectivity, the spherical shell must have enough surface area. If the surface area is too small, the magnetic tracks won't connect properly. Therefore, the area covered by holes must be less than 20%. To achieve the best results, we aim to maximize the number of holes while keeping this ratio at 80%. This simplifies the problem to a two-dimensional relationship between the number of hooks ( $M$ ) and the number of holes ( $N$ ). We then calculate the success rate of the configurations under various parameter settings. Specifically, we discretely select combinations where  $M$  takes values from 8 to 12 with a step size of 1, and  $N$  takes values from 280 to 320 with a step size of 10. For each combination, we randomly generate 5000 positions on the spherical shell and assess the success rate of the magnetic connections at these positions.

The experimental results are illustrated in Fig. 4, which presents the success rates for various values of  $M$  and  $N$ . The data reveal that the success rate is higher when

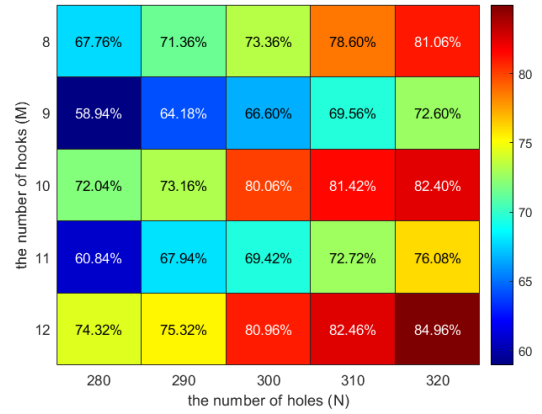


Fig. 4. Success rate of connectors with varying numbers of holes and hooks

the number of hooks is even compared to when it is odd. Specifically, the optimal performance is observed when  $N$  is approximately 300 and  $M \geq 10$ . Beyond this point, further increases in the number of hooks yield diminishing returns in success rate. This indicates a non-linear relationship between the number of hooks and the performance metric; after reaching a certain threshold, additional hooks do not substantially enhance the success rate.

Notably, due to the random nature of the projections, some variability in the specific data points is anticipated. Nonetheless, the overall trend remains evident. Considering practical aspects such as ease of manufacturing and processing, we have determined  $N = 300$  (corresponding to a hole diameter of 6 mm) and  $M = 10$  as the optimal parameters for our design. As a critical connection mechanism of the robot, the gripper must possess adequate load-bearing capacity once connected to the shell. Therefore, the material of the spherical shell must be both magnetic and sufficiently robust. To satisfy these requirements, we have selected Selective Laser Melting (SLM) technology for fabricating the spherical shell.

### C. Lifting Mechanism

Fig. 2(c) shows the design of the lifting mechanism. The core components include a screw rod motor and a bronze bushing. The screw rod motor provides the necessary power for the gripper's vertical movement, overcoming the magnetic attraction between the gripper and the spherical shell. The motor converts rotational motion into linear vertical movement through the screw rod, enabling precise up-and-down motion of the gripper. The self-locking feature of the screw rod maintains the gripper's position after lifting without requiring additional holding forces, ensuring stable operation. The bronze bushing, embedded at the upper and lower ends of the gripper, transmits the vertical movement and serves as a friction bearing, allowing smooth rotation of the gripper while connected. Additionally, the lifting mechanism can fully elevate other parts of the robot while the gripper remains connected, enabling passive rotation under specific conditions and enhancing the robot's flexibility and adaptability.

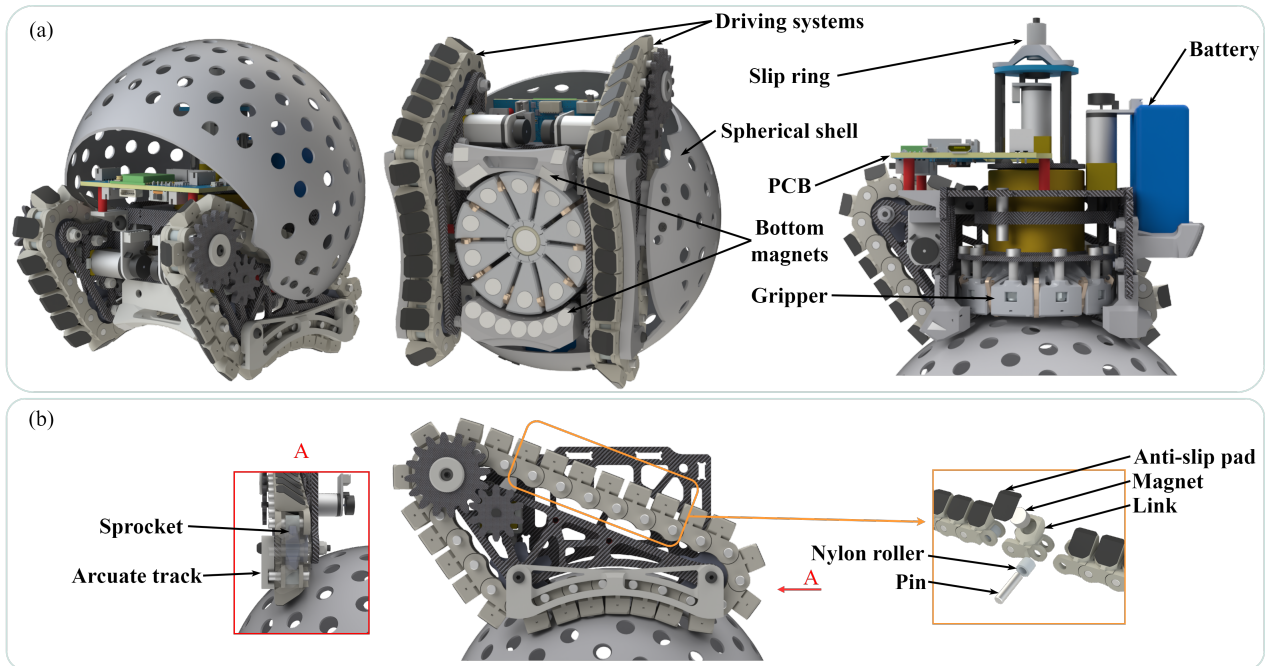


Fig. 5. (a) The overall structure of the SnailBot is displayed. (b) The mechanical structure of the chain driving system is introduced.

### III. RIGID MAGNETIC TRACK

The ability of MSRR systems to adapt their configuration in real-world applications is crucial. A robot's capability to quickly adjust its shape based on environmental needs is directly linked to the successful execution of tasks. However, frequent configuration changes also impose strict demands on the durability of the driving system. The new-generation SnailBot addresses these challenges by employing a chain magnetic track driving system. Compared to the previous generation, the new design introduces a arcuate track and a chain magnetic track, significantly enhancing the robot's mobility and surface adherence in spherical environments. Moreover, it extends the lifespan of the driving system, ensuring that the robot can continue to operate efficiently even during frequent configuration shifts.

Fig. 5 shows the SnailBot, with Fig. 5(b) illustrating the design of the chain magnetic track driving system. The chain magnetic track driving system in the new design demonstrates superior performance in motion execution. The chain is made from hard 3D-printed resin material, with links connected via movable joint segments, ensuring both flexibility and stability of the chain. Magnets embedded within the chain links are securely fixed using acrylic AB glue, ensuring their stability within the links. The contact surface of the chain with the sphere is covered with anti-slip patches to increase friction, improving the robot's adhesion and stability on the spherical surface. Inspired by [25], the arcuate track design ensures that the chain follows a predetermined trajectory on the sphere's surface, preventing detachment or misalignment during vertical climbing. The track is restricted to its intended path by a pin structure, enabling effective and continuous adhesion to the sphere's surface, thereby enhancing the robot's climbing and obstacle-

TABLE I  
MECHANICAL EXPERIMENT RESULTS

	Normal Force	Tangential Force	Torque
SnailBot-2	<100N	<50N	<3N·m
SnailBot-3	441.5N	>500N	4.2354N·m

crossing capabilities in complex terrains. Overall, the design optimizes the fit between the chain and the sphere and improves the compatibility between modules, enhancing the robot's performance across diverse application scenarios.

When designing and implementing the chain magnetic track driving system, the choice of chain link materials and the method of fixing the magnets are critical. The application of the chain magnetic track has significantly improved SnailBot's mobility and the lifespan of the driving system. Unlike the previous generation's flexible magnetic tracks, the resin material is more durable and maintains a stable shape. As the working surface of the magnetic track, the anti-slip patches play a crucial role in maintaining stability during the robot's movement. The introduction of arcuate tracks has also effectively enhanced SnailBot's climbing ability on the spherical shell. Additionally, maintenance of the driving system has been simplified, and by removing a single pin, the entire magnetic track can be easily detached. If part of the chain is damaged, only the corresponding links need to be replaced. This makes the repair process both efficient and cost-effective. Regular inspections of the chain, magnets, and related components are essential to ensure the system's long-term efficient operation.

The size optimization method of SnailBot is the same as in previous versions [24]. SnailBot weighs 680 g, with a length of 132.7 mm, a width of 120 mm, a height of 127.8 mm.

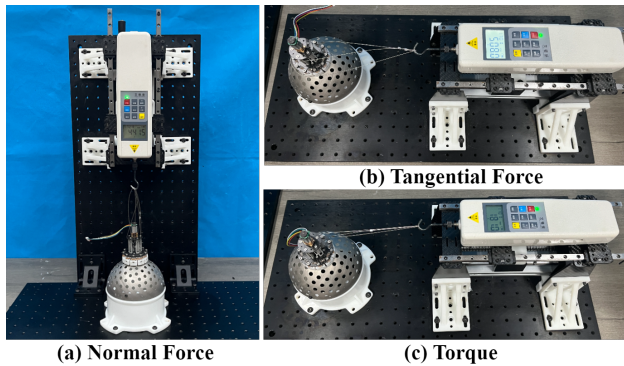


Fig. 6. Basic mechanical experiment of the connector.

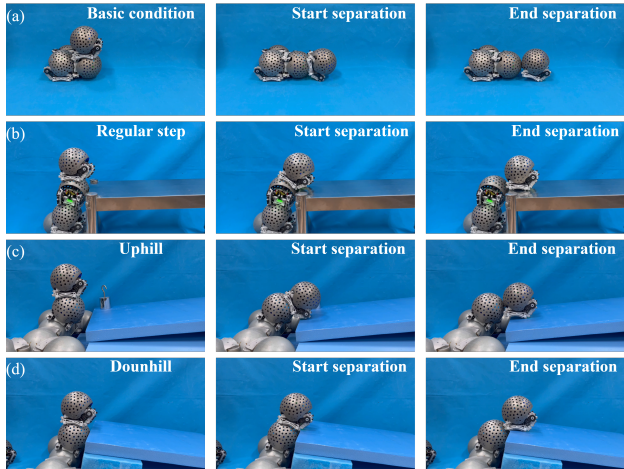


Fig. 7. The SnailBot can achieve stable separation under four different conditions.

## IV. EXPERIMENTS

### A. Connection Strength

The Fig. 6 illustrates the testing process, and the Table I shows the results. The tensile meter used in the experiment has a range of 500 N. In the experimental tests conducted on the improved connector, we observed a significant enhancement in connection strength. The new version of the connector exhibited superior performance across multiple dimensions, including normal force, tangential force, and torque.

### B. Basic Motion

The new driving system design has also shown significant improvements in basic motion capabilities (see Fig. 7). Compared to previous versions, the new driving system performs more reliably in module connection and separation actions. In earlier versions, separation between modules often encountered slippage, making it difficult to effectively disengage the modules. The new version addresses this issue, making the connection and separation actions smoother.

### C. Comprehensive Connectivity

The improved connector and chain magnetic track driving system provide robust support for stable connection and movement. The Fig. 8 illustrates the functionality of a transportation mechanism composed of modules. The new

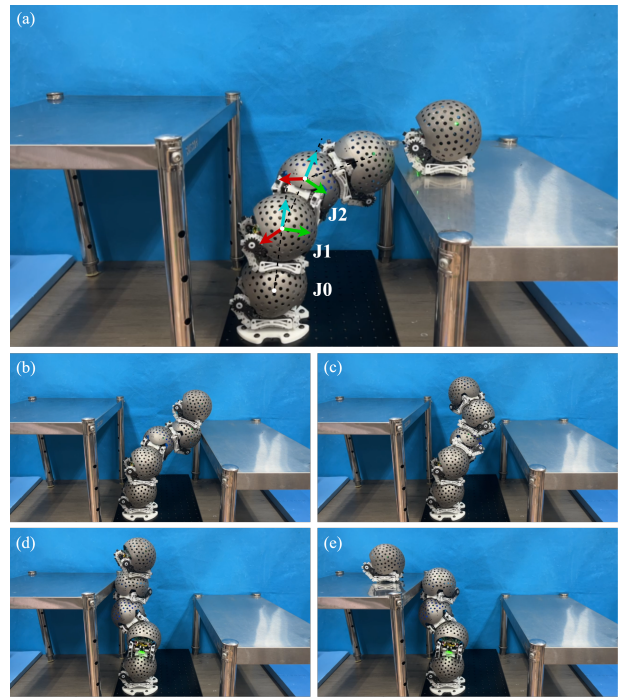


Fig. 8. A SnailBot is lifted and transported by other modules, crossing a lateral span of approximately 330 mm to reach another platform located at a relative height of 109 mm. The SnailBots in charge of transportation are stably connected to each other through the new connector.

connector enhances the connection strength between modules, improving the load-bearing capacity after connection. The driving system provides sufficient power for movement. During the transportation process, module J2 must overcome gravity to lift the SnailBot, a task that the previous version could not accomplish. The improved connection performance and stronger mobility ensure that SnailBot excels in applications requiring high load capacity, significantly enhancing its operational performance and reliability.

## V. DISCUSSION AND CONCLUSION

This paper presents an innovative design method that enhances SnailBot's connectivity and motion performance by combining a rigid freeform connector with a magnetic drive system. The specific design includes a multi-channel rope-driven gripper, a spherical shell with densely distributed holes, and a rigid chain magnetic driving system. This allows SnailBot to move stably on any surface and achieve strong connections. Experimental results validate the significant improvements in connection strength and motion reliability. The improved connector and track system not only enhance SnailBot's surface adaptability but also ensure stable operation in complex environments.

Although these designs improve SnailBot's performance, they also present challenges, such as increased manufacturing complexity and material costs. Future work will focus on optimizing the design to reduce costs and exploring its application in other robotic systems. Additionally, research will aim to improve adaptability and flexibility to handle more complex scenarios.

## REFERENCES

- [1] G. Liang, D. Wu, Y. Tu, and T. L. Lam, "Decoding modular reconfigurable robots: A survey on mechanisms and design," *The International Journal of Robotics Research*, 2024.
- [2] M. Shimizu and A. Ishiguro, "An amoeboid modular robot that exhibits real-time adaptive reconfiguration," in *2009 IEEE/RSJ International Conference on Intelligent Robots and Systems*. IEEE, 2009, pp. 1496–1501.
- [3] N. J. Wilson, S. Ceron, L. Horowitz, and K. Petersen, "Scalable and robust fabrication, operation, and control of compliant modular robots," *Frontiers in Robotics and AI*, vol. 7, p. 44, 2020.
- [4] A. Nilles, S. Ceron, N. Napp, and K. Petersen, "Strain-based consensus in soft, inflatable robots," in *2022 IEEE 5th International Conference on Soft Robotics (RoboSoft)*. IEEE, 2022, pp. 789–794.
- [5] G. Liang, H. Luo, M. Li, H. Qian, and T. L. Lam, "FreeBOT: A freeform modular self-reconfigurable robot with arbitrary connection point-design and implementation," in *2020 IEEE/RSJ International Conference on Intelligent Robots and Systems (IROS)*. IEEE, 2020, pp. 6506–6513.
- [6] T. L. Lam and G. Liang, "Self-reconfigurable robot module and self-reconfigurable robot," Jul. 2 2024, US Patent 12,023,809.
- [7] P. Swisler and M. Rubenstein, "Fireant3d: a 3d self-climbing robot towards non-latticed robotic self-assembly," in *2020 IEEE/RSJ International Conference on Intelligent Robots and Systems (IROS)*. IEEE, 2020, pp. 3340–3347.
- [8] V. Zykov, E. Mytilinaios, M. Desnoyer, and H. Lipson, "Evolved and designed self-reproducing modular robotics," *IEEE Transactions on robotics*, vol. 23, no. 2, pp. 308–319, 2007.
- [9] S. Hauser, M. Mutlu, and A. J. Ijspeert, "Kubits: Solid-state self-reconfiguration with programmable magnets," *IEEE Robotics and Automation Letters*, vol. 5, no. 4, pp. 6443–6450, 2020.
- [10] C. Liu, Q. Lin, H. Kim, and M. Yim, "Smores-ep, a modular robot with parallel self-assembly," *Autonomous Robots*, vol. 47, no. 2, pp. 211–228, 2023.
- [11] D. Zhao and T. L. Lam, "Snailbot: a continuously dockable modular self-reconfigurable robot using rocker-bogie suspension," in *2022 International Conference on Robotics and Automation (ICRA)*. IEEE, 2022, pp. 4261–4267.
- [12] J. W. Romanishin, K. Gilpin, S. Claici, and D. Rus, "3d m-blocks: Self-reconfiguring robots capable of locomotion via pivoting in three dimensions," in *2015 IEEE International Conference on Robotics and Automation (ICRA)*. IEEE, 2015, pp. 1925–1932.
- [13] G. Liang, Y. Tu, L. Zong, J. Chen, and T. L. Lam, "Energy sharing mechanism for a freeform robotic system-freebot," in *2022 international conference on robotics and automation (ICRA)*. IEEE, 2022, pp. 4232–4238.
- [14] M. W. Jorgensen, E. H. Ostergaard, and H. H. Lund, "Modular atron: Modules for a self-reconfigurable robot," in *2004 IEEE/RSJ International Conference on Intelligent Robots and Systems (IROS)(IEEE Cat. No. 04CH37566)*, vol. 2. Ieee, 2004, pp. 2068–2073.
- [15] W.-M. Shen, R. Kovac, and M. Rubenstein, "Singo: a single-end-operative and genderless connector for self-reconfiguration, self-assembly and self-healing," in *2009 IEEE international conference on robotics and automation*. IEEE, 2009, pp. 4253–4258.
- [16] H. Wei, Y. Chen, J. Tan, and T. Wang, "Sambot: A self-assembly modular robot system," *IEEE/ASME transactions on mechatronics*, vol. 16, no. 4, pp. 745–757, 2010.
- [17] C. H. Belke and J. Paik, "Mori: a modular origami robot," *IEEE/ASME Transactions on Mechatronics*, vol. 22, no. 5, pp. 2153–2164, 2017.
- [18] Y. Zhu, J. Zhao, X. Cui, X. Wang, S. Tang, X. Zhang, and J. Yin, "Design and implementation of ubot: A modular self-reconfigurable robot," in *2013 IEEE International Conference on Mechatronics and Automation*. IEEE, 2013, pp. 1217–1222.
- [19] J. Neubert, A. Rost, and H. Lipson, "Self-soldering connectors for modular robots," *IEEE Transactions on Robotics*, vol. 30, no. 6, pp. 1344–1357, 2014.
- [20] R. F. M. Garcia, J. D. Hiller, K. Stoy, and H. Lipson, "A vacuum-based bonding mechanism for modular robotics," *IEEE Transactions on Robotics*, vol. 27, no. 5, pp. 876–890, 2011.
- [21] Y. Tu, G. Liang, and T. L. Lam, "Freesn: A freeform strut-node structured modular self-reconfigurable robot-design and implementation," in *2022 International Conference on Robotics and Automation (ICRA)*. IEEE, 2022, pp. 4239–4245.
- [22] Y. Tu and T. L. Lam, "Configuration identification for a freeform modular self-reconfigurable robot-freesn," *IEEE Transactions on Robotics*, 2023.
- [23] G. Liang, L. Zong, and T. L. Lam, "DISG: Driving-integrated spherical gear enables singularity-free full-range joint motion," *IEEE Transactions on Robotics*, 2023.
- [24] D. Zhao, H. Luo, Y. Tu, C. Meng, and T. L. Lam, "Snail-inspired robotic swarms: a hybrid connector drives collective adaptation in unstructured outdoor environments," *Nature Communications*, vol. 15, no. 1, p. 3647, 2024.
- [25] J. Hu, X. Han, Y. Tao, and S. Feng, "A magnetic crawler wall-climbing robot with capacity of high payload on the convex surface," *Robotics and Autonomous Systems*, vol. 148, p. 103907, 2022.